AD_____
(Leave blank)

Award Number:
W81XWH-08-1-0192

TITLE:
INCORPORATING FUNCTIONAL IMAGING INFORMATION TO rpFNA ANALYSIS FOR BREAST CANCER DETECTION IN HIGH-RISK WOMEN

PRINCIPAL INVESTIGATOR:
Kristy L. Perez

CONTRACTING ORGANIZATION:
Duke University
Durham, NC 27706

REPORT DATE:
March 2009

TYPE OF REPORT:
Annual Summary

PREPARED FOR: U.S. Army Medical Research and Materiel Command
Fort Detrick, Maryland 21702-5012

DISTRIBUTION STATEMENT: (Check one)

X Approved for public release; distribution unlimited

☐ Distribution limited to U.S. Government agencies only; report contains proprietary information

REPORT DOCUMENTATION PAGE

Form Approved
OMB No. 0704-0188

1. REPORT DATE *(DD-MM-YYYY)*	2. REPORT TYPE	3. DATES COVERED *(From - To)*
31-03-2009	Annual Summary	01 MAR 2008 - 28 FEB 2009

4. TITLE AND SUBTITLE
Incorporating Functional Imaging Information into rpFNA

Analysis for Breast Cancer Detection in High Risk Women

5a. CONTRACT NUMBER

5b. GRANT NUMBER
W81XWH-08-1-0192

5c. PROGRAM ELEMENT NUMBER

6. AUTHOR(S)
Kristy Perez

Email: kristy.perez@duke.edu

5d. PROJECT NUMBER

5e. TASK NUMBER

5f. WORK UNIT NUMBER

7. PERFORMING ORGANIZATION NAME(S) AND ADDRESS(ES)

Duke University
Office of Sponsored Programs
Box 104135
Durham, NC 27708
E-mail: klp14@duke.edu

8. PERFORMING ORGANIZATION REPORT NUMBER

9. SPONSORING / MONITORING AGENCY NAME(S) AND ADDRESS(ES)
US Army Medical Research and Material Command
Fort Detrick, MD 21702-5012

10. SPONSOR/MONITOR'S ACRONYM(S)

11. SPONSOR/MONITOR'S REPORT NUMBER(S)

12. DISTRIBUTION / AVAILABILITY STATEMENT
Approved for public release; distribution unlimited

13. SUPPLEMENTARY NOTES

14. ABSTRACT
The overall goal of this work is to correlate the imaging information from the dual-modality, dedicated single photon emission computed tomography (SPECT) and computed tomography device with the results of random periareolar fine needle aspiration (rpFNA) in women at high risk for breast cancer. To maximize the information gained from this collaborative study, the whole breast will be imaged prior to rpFNA and the needles will be imaged after aspiration has been collected. In this first year of work, efforts have been concentrated on understanding the SPECT image signal and correcting for artifacts, attenuation and scatter to the reconstructed SPECT images. Additionally, preliminary data was collected to investigate the potential of imaging the radioactive rpFNA needles with our current SPECT camera. Other aspects of the training program have been initiated, including attending local and international conferences, shadowing breast cancer related procedures in the hospital, and drafting papers for peer review.

15. SUBJECT TERMS
Nuclear Medicine Imaging, SPECT, Molecular Breast Imaging, Mammotomography, rpFNA

16. SECURITY CLASSIFICATION OF:			17. LIMITATION OF ABSTRACT	18. NUMBER OF PAGES	19a. NAME OF RESPONSIBLE PERSON
a. REPORT	b. ABSTRACT	c. THIS PAGE	Unlimited	21	Kristy Perez
Unclassified	Unclassified	Unclassified			19b. TELEPHONE NUMBER *(include area code)* 919-684-7943

Table of Contents

A. Introduction

The overall goal of this work is to correlate the imaging information from our dual-modality, dedicated single photon emission computed tomography (SPECT) and computed tomography (CT) device with results of random periareolar fine needle aspiration (rpFNA) in women at high risk for breast cancer. To maximize the information gained from this collaborative study, the whole breast will be imaged prior to rpFNA and the rpFNA needles will be imaged directly following aspiration. In this first year of work, efforts have been concentrated on understanding the SPECT signal and correcting for artifacts, attenuation and scatter to the reconstructed SPECT images. Additionally, preliminary data was collected to investigate the potential of imaging the radioactive rpFNA needles with our current SPECT camera. Other aspects of the training program have been initiated, including attending local and international conferences, shadowing breast cancer related procedures in the hospital, and drafting papers for peer review.

B. Body

The Statement of Work and proposed timeline are included in Appendix A. For Year 1, the tasks outlined preparations for and initiation of collecting and correlating patient SPECT-CT and rpFNA data. Although preparations are underway and a more detailed understanding of the data acquired has been studied, each of these tasks are continuing and patient data has not yet begun.

Task 1: Acquire IRB approval

Task 1(a): Participate on writing IRB protocol for FMT imaging in a high risk patient cohort.

The institutional review board (IRB) protocol for this study has been drafted and is awaiting submission. The IRB will be submitted when Tasks 2(a)-(c) and 3(a)-(b) are more nearly completed. Along with my advisor, we concluded that once the whole breast quantification was more clearly established (Task 3(b)), we would submit the IRB protocol for review.

Task 2: Evaluate radioactive needles for guided histology

Task 2(a): Design shielded holder or sleeves to image the individual signal from each biopsy needle.

Task 2(c): Use phantoms to test designed holder, and modify as necessary.

Calculations were performed using theoretical values for scatter for a variety of materials of which a needle shield could potentially be made (Figure 1). A preliminary design of the shield was constructed of a 0.64 cm lead sheet available in the lab to test the design concept and material. A 4 min planar image of a 25-gauge needle containing 8 μCi of aqueous ^{99m}Tc was acquired in two hour intervals with our 16x20 cm^2 CZT gamma camera. After about 48 hours, the decaying activity approached clinically estimated quantities for this study, or about 60

Material	σ	μ	σ/μ
Lead	0.096	2.27	0.042203
Stainless Steel	0.122	0.222	0.548155
Acrylic	0.146	0.147	0.993197
Copper	0.119	0.222	0.536036
Aluminum	0.129	0.135	0.955556
Tungsten	0.098	2.044	0.048102

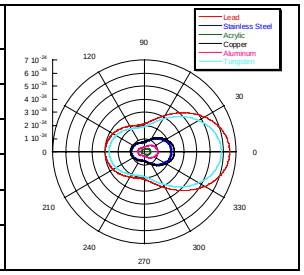

FIGURE 1: (RIGHT) Polar plot of the predicted probability of photon scattering angles from an incident 140 keV photon, according to the Klein-Nishina Distribution for different proposed needle shielding materials of varying atomic number. The relative magnitude of the curves indicate that lead would have a better chance of backscattering 140keV photons than acrylic, if the photons Compton scattered in the material. However, as shown in the table (LEFT), since the Compton cross section for interaction is greater in lower Z substances, another material may backscatter more photons resulting in a higher count rate than lead. The other listed materials in the table are being further investigated, with a more finely designed shielding device for this needle imaging procedure.

nCi. Experiments to determine the minimum detectable activity included imaging with an open energy window versus a ±4% energy window, and with and without a parallel hole collimator to identify spatial information along the length of the needle.

Although the activity in the base of the syringe is greater than along the needle length, the outline of the residual activity in the needle can be discerned above background levels both with and without the lead shield and without the camera collimator (Figure 2). Images with the camera's parallel hole medium efficiency collimator were acquired to evaluate the differences in the overall number of counts obtained, and also to determine the ability to better discern the spatial information along the length of the needle (Figure 3). Studies with the lead shield covering the detector face show an increase in the mean counts detected over those detected without the lead with an open energy window, however, this effect was not statistically significant (Figure 4). As expected, the mean counts collected in a ±4% energy window with and without the lead shield were approximately equal because the backscatter energies would range from 91 to 110 keV, well below the 134 keV cutoff. The background CR is higher for an open energy window, even with the lead sheet covering the detector, than for a ±4% energy window. From these images, it seems that some simple form of collimation that has high efficiency may be warranted. Various collimator thicknesses will therefore be evaluated from the 2.54 cm thick collimator used here, to increasingly shorter ones.

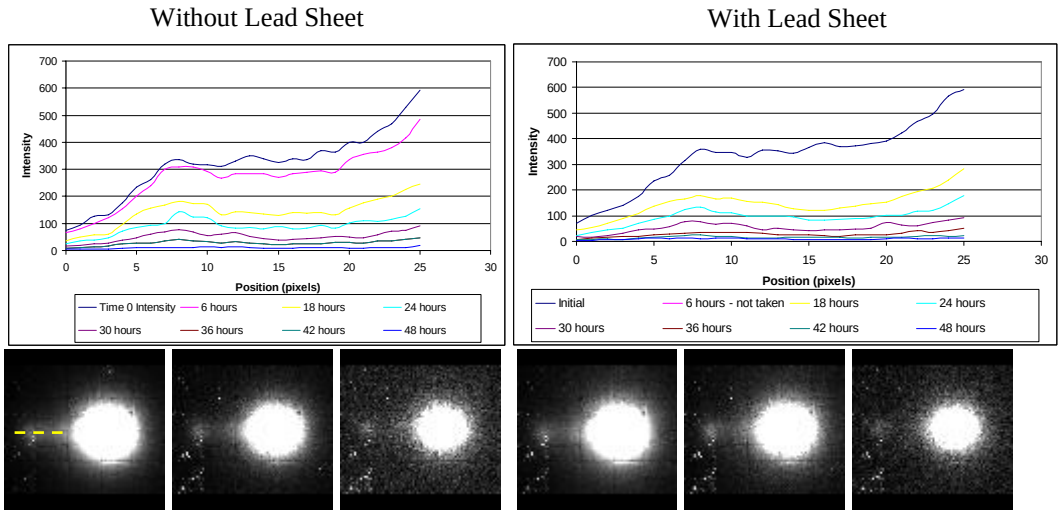

FIGURE 2: (TOP, LEFT&RIGHT) Line profiles (drawn along the yellow dotted line in the left bottom image) from the open energy window and no collimator data collected depict the potential for radiochromatography with the radioactive needle. These line profiles pertain to images acquired without using lead for reflective material. (BOTTOM, LEFT) Three serial images acquired with an open energy window. The images are from left to right, acquired 6 hours after the start, 18 after the start, and 48 hours after they start. (BOTTOM, RIGHT) Planar images of the needle and syringe after decaying for 18 hours, 26 hours and 48 hours.

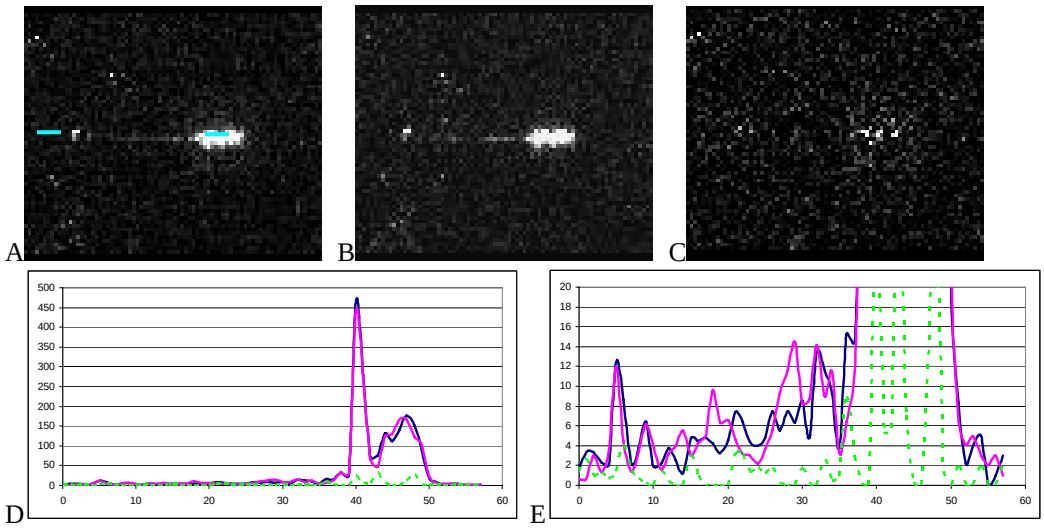

FIGURE 3: (A) and (B) are planar images of a 25 gauge fine needle filled with 8μCi of ^{99m}Tc acquired for 4min with an open energy window (full spectrum) and the collimator attached. In image A, a lead sheet covers the needle and entire detector face. In image B, the needle is imaged without the lead sheet in place. (C) The difference image of A minus B. (D) Line profiles drawn through the needle (along the line of the yellow hash mark in (A)). The dark blue line represents the profile through image A; the magenta line, image B; and the green dotted line, image C. The large peaks are due to radioactivity concentrated in the syringe as opposed to the fine needle. (E) The same plot profile displayed on a scale such that the variations of detected activity in the needle can be distinguished.

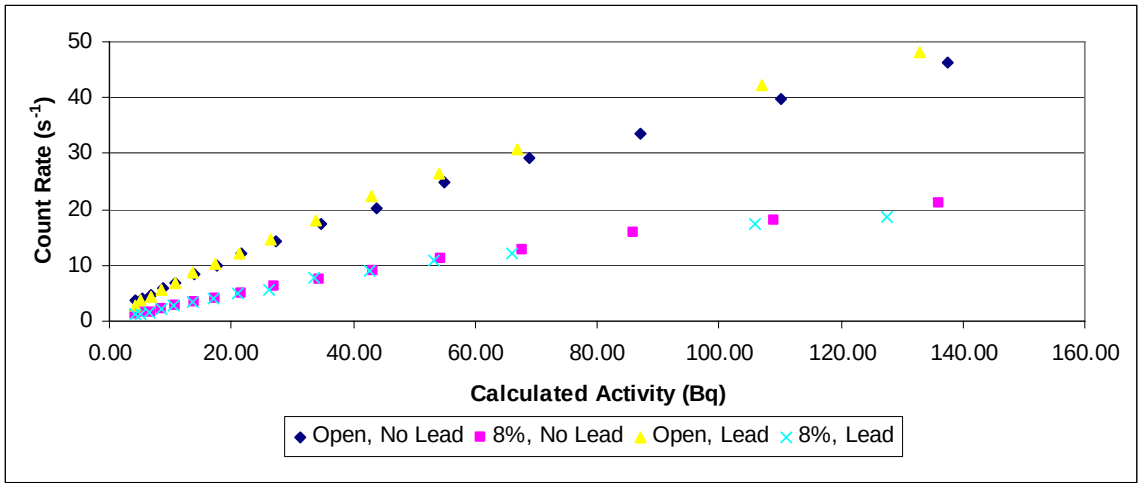

FIGURE 4: Plot of the measured count rate in the needle as a function of the amount of calculated activity (based on exponential decay from initially measured activity) over ~30 hours (5 half-lives). As expected, the parameters are proportional and trend toward an intercept of zero. For an open energy window, the lead sheet increases the count rate for (relatively) large activities, however as the activity approaches zero the lead sheet does not seem to have as big of an effect on the count rate. As expected, the count rate in the +/-4% energy window is not impacted by the presence of the lead sheet because the backscattered photons (91-110keV) are outside the windowed energy range (134-146keV).

Further analysis will help indicate if needle radiochromatography could be performed along with the cellular analysis for fine needle aspiration in high risk women. However very low count rates and therefore noisy data (simulating calculated clinical count rates) makes rigorous analysis and comparison of the shields difficult. Therefore, it has been decided that GEANT4, a computer modeling and simulation code, should be used to first test different design ideas in a controlled setting. Installing GEANT4 required a systems update for our computer operating system and downloading supporting software, such as a new C++ complier. These tasks have been completed and I am currently learning the GEANT4 software.

Task 3: Optimize patient imaging and biopsy protocol.

Task 3(a): Investigate how the dedicated SPECT imaging and biopsy procedures can be optimally integrated to minimize the patient scan times.

The rpFNA procedure requires about 30 minutes and the SPECT-CT scan requires about 40 minutes to complete. The ideal scenario would minimize the procedural time of the two methods for the convenience of the volunteer. Through discussions with Dr. Seewaldt and Dr. Tornai, it has been decided that the best initial approach will be to do both the imaging and rpFNA collection in our lab, minimizing volunteer travel and setup time. Moving our equipment is a costly and time consuming endeavor with technical issues of radiation safety and electrical power requirements. However, relocating the rpFNA procedure requires primarily a private, comfortable environment. Sterile needles, syringes and other necessary items can be brought to our lab for the procedure for this limited patient study.

Task 3(b): Investigate how the information gained with SPECT imaging can be incorporated into the biopsy procedure.

Correlating imaging information with the Masood cytology score could result in valuable information for the high risk population. Mapping functional changes along with histological analysis of cells could give useful information about a woman's short term cancer risk. However, the imaging signal should be well understood and, hopefully, quantitative to provide objective evaluation and easy comparisons between the very different data types. Further exploration of the imaging data has been completed, including understanding the effects of

out of field of view activity, i.e. contamination from the heart and liver, and correcting the signal for degrading effects, such as attenuation and scatter, making a quantifiable image to compare with cellular sampling.

To investigate the effects of the hepatic and cardiac contamination, anthropomorphic phantoms were filled with clinical concentrations of radioactivity. Data were acquired with sequential tilted parallel beam (TPB) trajectories with polar angles of 15°, 20°, 25°, 30°, 40°, 45°, 50° and 60°. Figure 5 displays a plot of the counts per projection as a function of azimuthal position. Using TPB 15° as a baseline of normalized contamination-free counts for comparison, there are azimuthal positions where large polar tilt angles (40° – 50°) maybe used to image into the chest wall without directly viewing the heart or liver. This indicates that the camera trajectory could encompass large polar angles where the camera might be under the organs and looking up towards the pectoral muscle. Data collected here would not contain direct background counts from the heart or liver. The bounds of the camera's polar angles for the left breast, derived from minima in the counts per projection curve (Figure 5), shows that the trajectory is most stringently limited in the upper right quadrant (Figure 6).

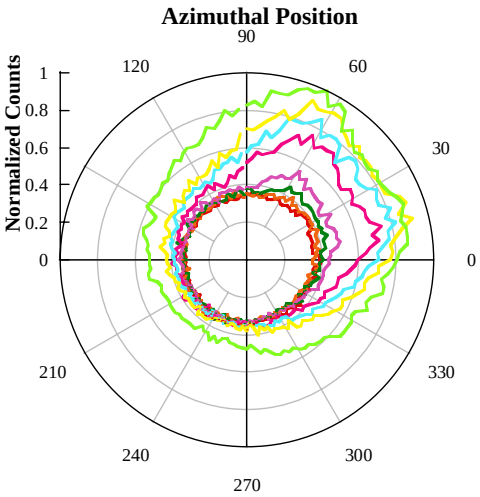

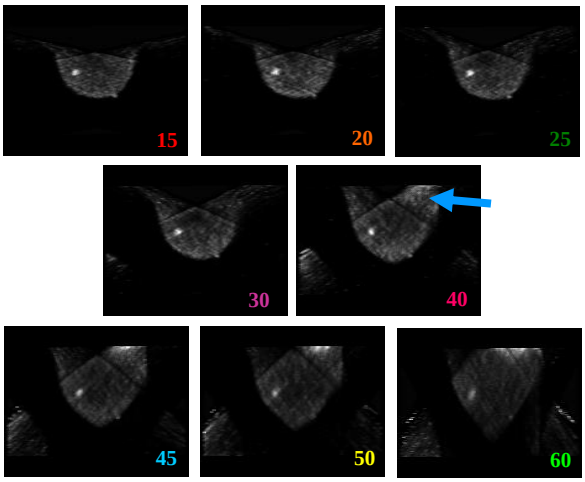

FIGURE 5: (LEFT) Plot of counts per projection acquired for sequential TPB scans. The plot line color corresponds to the colored tilt angle in the images at Right. Data are displayed as a solid line. The curves deviate in the upper right quadrant due to increased counts when viewing the heart and liver. (RIGHT IMAGES) Three summed transverse slices of second iteration reconstructed images. As the polar angle increases (# in bottom right corner), the imaged volume of the chest wall and axilla increases. The heart and liver activity presents as a bright region (arrow) and shape distortion occurs at ~40°.

Slices from the corresponding reconstructed images show that as the trajectory deviates from the TPB 15° baseline, increased activity appears in the chest wall region (Figure 5). The incomplete sampling in these acquisitions manifests itself in the image as breast shape distortion (an elongation and increasingly triangular appearance) and contamination (activity in the lower corners of the images) [1, 2].

Additionally, a variety of acquisition trajectories were tested using a mulitple starting points to simulate different sampling strategies. The reconstructed images in Figure 7 show the difference resulting from the variety of trajectories used. One trajectory, TPB 45°, which has been proven in patient studies to be an advantageous and useful data collection scheme, surprisingly did not yield a reconstructed image in which the lesion could be visualized. However, the other data acquisition trajectories yielded images in which the lesion could be visualized.

The acquisitions which produced the best signal to noise ratio (SNR) and contrast (Table 1) were the projected sinusoid (PROJSINE) starting at 90° (Figure 7),

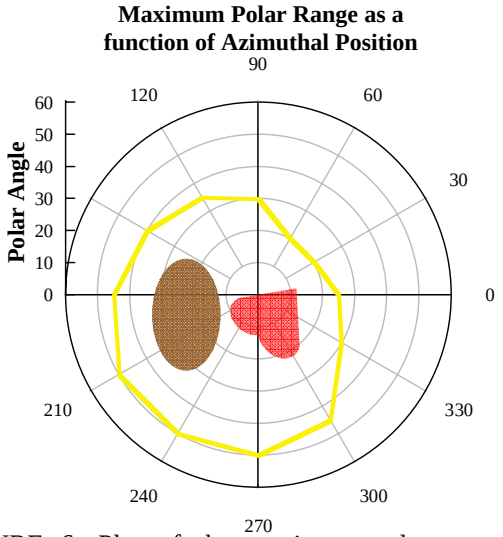

FIGURE 6: Plot of the maximum polar range as a function of the azimuthal position for the left breast given minimum (i.e. breast only) counts obtained at these azimuthal and polar views. If the camera trajectory exceeds this range then direct views of the heart and liver will result.

where the camera had minimum view into the heart and liver, and TPB 15°. Circle plus arc (CPA) starting at 135° had a similarly high contrast, but the SNR was not different than in the other acquired images. The equal SNRs were an unexpected result. Indeed other trajectories, such as PROJSINE starting at 135°, also did not have the high SNR or contrast as expected. While the optimal acquisition trajectory should have many close and direct views of the lesion, other factors, such as breast size, may warrant consideration in deciding the best trajectory. Of particular note, moreover, is that the complex trajectories yield better results than VAOR alone.

Table 1: Table of SNR and contrast values in the coronal plane for the second iteration of reconstructed images

Trajectory	SNR	Contrast
VAOR	**3.3**	**4.3**
TPB 15°	**6.2**	**10.7**
TPB 45°	**0.6**	**1**
CPA arcing at 90°	**3.2**	**6.6**
CPA arcing at 60°	**4.8**	**7.4**
PROJSINE	**6.9**	**10**
PROJSINE at 60°	**2.2**	**4**
PROJSINE at 135°	**3.1**	**5.6**
SADDLE	**3.7**	**7.2**
CPA arcing at 135°	**4.8**	**11.4**

Acquisition trajectories can be made to avoid direct views of the heart and liver by limiting the camera's polar angular range over the azimuthal acquisition range (Figure 6). A nearly infinite number of trajectories can be constructed within the bounds of the maximum polar tilt to avoid the heart and liver and remove the associated artifact while still imaging the breast and chest wall. For quantitative imaging, as in previous studies [5], the heart and liver activity would probably need to be accounted for to achieve accurate lesion activity values.

Quantification of radiotracer uptake in focal lesions and the entire breast volume will be valuable information to directly and objectively compare to the cellular analysis of rpFNA. Physical processes and, with systems capable of 3D trajectories, reconstruction artifacts can yield an incorrect absolute activity of the tracer. Differences in the obtained activity value from each trajectory are investigated to determine if the acquisition trajectory can be used for quantification. For these experiments, a fillable 600mL breast and 2.3mL lesion phantoms containing aqueous ^{99m}Tc pertechnetate were imaged with the dedicated dual-modality SPECT-CT scanner. SPECT images were collected with various 3D acquisitions including vertical axis of rotation (VAOR), TPB 45°, and PROJSINE trajectories. Collimator and detection efficiencies of the SPECT camera were incorporated into the OSEM iterative reconstruction. Attenuation correction was implemented using a uniform attenuation coefficient matrix, but in subsequent trials will be done with scaled volumetric CT images obtained from our system. In addition, a Compton Window scatter correction method was applied with an empirically determined k value of 0.3 and a scatter window ranging from 113 to 133 keV, abutting and below the 8% photopeak window. Additional scatter correction techniques are being investigated to determine if the quantification accuracy can be increased. This first approach uses a line source to estimate a scaling factor of 0.07, which can be used to correct reconstructed data to activity. The resulting calculated lesion activity in the image was found to be within 20.5% (+/- 9.9%) of the dose calibrator measured activity value across the different trajectories (Table 2). The scaled breast background values were double the dose calibrator measured activity value indicating that further investigation of the linearity of the method is needed. Additionally, fused CT images can be used to define regions of interest (ROI) to be applied to SPECT images (Figure 8), which could lead to better quantification by more accurately defining the ROI. As far as we are aware, this is the first

time that absolute quantification has been applied to SPECT data acquired with non-traditional, non-circular trajectories.

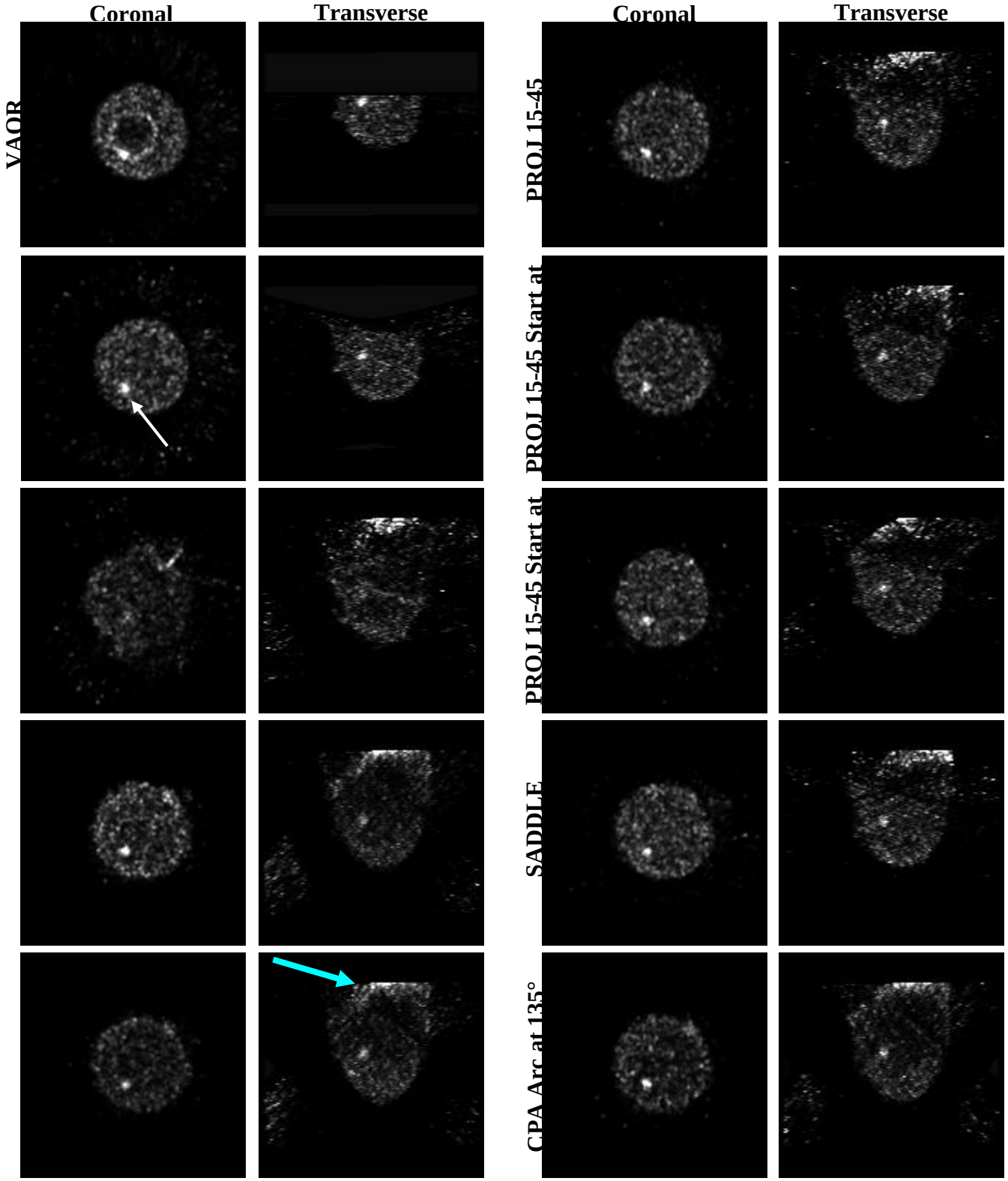

FIGURE 7: Four summed second iteration coronal and transverse reconstructed slices smoothed with a Gaussian kernel acquired with a variety of trajectories imaging a 2.1 mL lesion in the inferior, lateral quadrant of a 1730 mL breast phantom. The white arrow points to the lesion location in the TPB 15° image. The aqua arrow points to the increase activity due to the heart and the liver, which is apparent in several of the reconstructed images. Note: The lesion is not visualized in the image acquired with the TPB 45° trajectory.

Table 2: Comparison of dose calibrator measured activity and measured activity in an image ROI in the breast and lesion phantoms. The ROIs encompassed areas in the lesion and breast background with 6 summed slices in the vertical axis of rotation (VAOR) and projected sine wave (PROJSINE) acquisition studies and 9 summed slices in the tilted parallel beam (TPB) study (summing all planes containing hot lesion). For the lesion, VAOR measurements were within 10% of the dose calibrator values, while PROJSINE and TPB measurements were within 30%. For the breast background, the scaled values were approximately double the dose calibrator values.

Acquisition	ROI Location	Quantified Activity from Reconstructed Image (uCi/mL)	Dose Calibrator Activity (uCi/mL)	% Error
VAOR	Lesion	30.1	33.1	9.07
	Breast	10.0	5.0	-99.52
PROJSINE	Lesion	23.1	31.7	27.08
	Breast	8.4	4.8	-74.84
TPB	Lesion	22.8	30.5	25.36
	Breast	10.2	4.6	-121.15

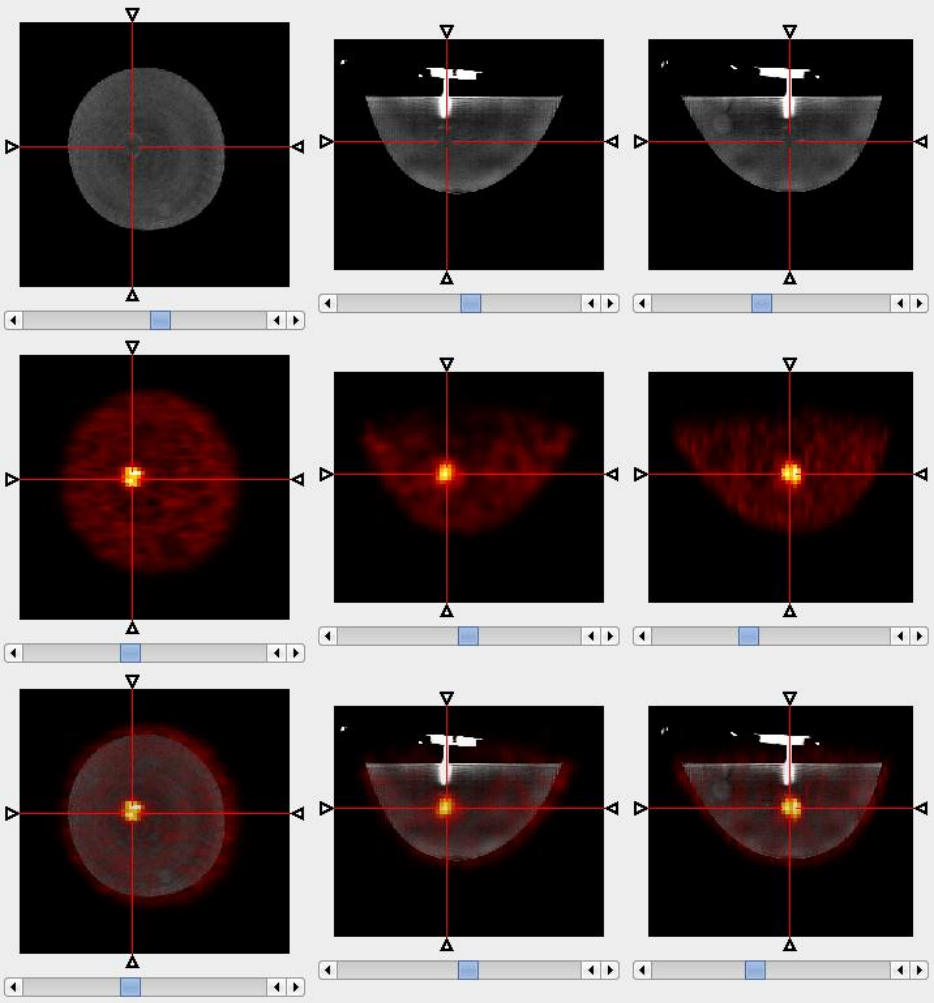

FIGURE 8: Cross sectional slices of reconstructed, scatter corrected CT (TOP) and attenuation and scatter corrected SPECT (MIDDLE) phantom data and the registered and fused images (BOTTOM). The data is shown in coronal (LEFT), transverse (CENTER) and sagittal (RIGHT) slices. At the center of the red crosshairs, the outer acrylic shell of the fillable lesion can be seen in the CT image, and a hot spot of activity can be seen in the SPECT image.

Task 4: Complete other aspects of breast cancer training program

Task 4(a): Shadow and observe clinical and diagnostic side of breast cancer imaging.

I have shadowed multiple technologists in the mammography suite encompassing procedures to image patients with both digital and film techniques, to complete daily, weekly, monthly and yearly quality assurance

of acquiring and processing images, and with the physicians to read and diagnose images. I also completed the procedure for the annual quality assurance of a mammography unit and now understand the aspects of diagnostic imaging which need to be tested in order to ensure the safety of the patient and the reliability of the diagnosis.

Additionally, I shadowed a nurse performing the rpFNA procedure and spoke with the patients undergoing the procedure. I gained an understanding of how 1) the patients are prepared for the procedure, 2) the needle aspirations are collected, and 3) the samples are prepared and processed. This experience has given me insight to develop the integration procedures for the SPECT-CT and rpFNA combined studies germane to this award. I was able to address some of the concerns of the nurses regarding their potential radioactive dose. Also, it became clear that for the first set of patients, the rpFNA procedure would have to be completed at our current lab because relocating our equipment into their suite would be logistically difficult. We initiated discussions about what steps would need to be taken to do their procedure in our lab space.

Task 4(c): Attend and present at local seminars and conferences

I have attended many local conferences and seminars, including but not limited to Duke SPORE Breast Cancer meetings, medical physics and nuclear medicine journal clubs, Duke sponsored Tomosynthesis Imaging Symposium 2009 that included breast imaging, and Southeastern American Association of Physicists in Medicine (SEAAPM) meeting held in Chapel Hill, NC. I have presented at the nuclear medicine journal club and the medical physics weekly seminar.

Task 4(d): Attend international conferences

I attended and gave an oral presentation at the *4th International Workshop on the Molecular Radiology of Breast Cancer* in Dresden, Germany in October 2008. The presentation was well received at the workshop, and I obtained useful feedback and suggestions on this work. I also attended the *IEEE Nuclear Science Symposium and Medical Imaging Conference* there.

C. Key Research Accomplishments

Task 1, Task 2(a)-(c), and Task 3(a)-(b) were to be completed in Year 1. Task 2(a)-(b), designing and constructing a needle shield/holder, will rely on the findings from the GEANT4 simulations, and thus have been initiated. Tasks 1, 2(c), and 3(a)-(b) have been initiated, but are incomplete at this time. Progress has been made for each task as follows:

- An IRB protocol has been drafted and is awaiting submission.
- Initial data to test the detector system's ability to image low activity rpFNA needles has been collected with insufficient results. Another method has been identified to better examine this idea and is in progress.
- Investigated effects of cardiac and hepatic radioactive background contamination on the breast image. This work was presented at the *2008 Molecular Radiology of Breast Cancer Workshop* (Appendix B).
- The Compton Window Scatter Correction Method has been investigated and implemented. Initial results with this scatter correction method indicate that it is insufficient to produce quantitative images, though another means of implementing it are under investigation.
- Clinical shadowing of mammography and rpFNA procedures has been completed. The rpFNA shadowing led to fruitful discussions pertinent to Task 3(a)-(b).

Related

This original DOD grant application along with data collected during the first year of the award was used as the basis for my preliminary doctoral proposal, "Incorporating Functional Imaging Information into Random

Periareolar Fine Needle Aspiration Analysis in Women at High Risk for Breast Cancer," which was accepted by my dissertation committee on August 28, 2008.

D. Reportable Outcomes

Conference Proceedings

P Madhav, SJ Cutler, DJ Crotty, **KL Perez**, RL McKinley, L Wilke, TZ Wong, MP Tornai. "Pilot Patient Studies Using a Dedicated Dual-Modality SPECT-CT System for Breast Imaging." Presented at the *2008 American Association of Physicists in Medicine Annual Meeting*, Houston, Texas 17-31 Jul 2008, and published in *Med. Phys.* **35**(6):2894.

DJ Crotty, SJ Cutler, RL McKinley, P Madhav, **KL Perez**, MP Tornai. "Improved Chest Wall Imaging through Combined Complex Trajectories in Dedicated Dual Modality SPECT-CT Breast Molecular Imaging." Presented at *4th International Workshop on the Molecular Radiology of Breast Cancer*, Dresden, Germany, 20-21 October, 2008, and published in *2008 IEEE Nuclear Science Symposium & Medical Imaging Conference Record*, 5650-5665.

SJ Cutler, **KL Perez**, P Madhav, MP Tornai. "Comparison of 2D Scintimammography and 3D Dedicated Breast SPECT Using a Compressible Breast Phantom and Lesions of Varying Size and Tracer Uptake." Presented at *4th International Workshop on the Molecular Radiology of Breast Cancer*, Dresden, Germany, 20-21 October, 2008, and published in *2008 IEEE Nuclear Science Symposium & Medical Imaging Conference Record*, 5640-5646.

KL Perez, SJ Cutler, P Madhav, MP Tornai. "Novel Patient Optimized Acquisition Trajectories for Dedicated Breast SPECT Imaging." Presented at *4th International Workshop on the Molecular Radiology of Breast Cancer*, Dresden, Germany, 20-21 October, 2008, and published in *2008 IEEE Nuclear Science Symposium & Medical Imaging Conference Record*, 5629-5634.

In Preparation for Publication

KL Perez, SJ Cutler, P Madhav, MP Tornai. "Characterizing the Contribution of Cardiac and Hepatic Uptake in Dedicated Breast SPECT using Tilted Trajectories." Preparing for submission to *Physics in Medicine and Biology*.

SJ Cutler, **KL Perez**, MP Tornai. "3D Contrast-Detail Analysis for Dedicated Emission Mammotomography." Submitted to *Physics in Medicine and Biology*.

Funding

Received Conference Travel Fellowship from Duke University Graduate School to help pay the costs for travel to Dresden, Germany for the *2008 Molecular Radiology of Breast Cancer Workshop* and *IEEE Nuclear Science Symposium and Medical Imaging Conference.*

Received a registration fee waiver for the *2008 Molecular Radiology of Breast Cancer Workshop* to attend the workshop and present my results from my submitted and accepted abstract.

E. Conclusions

In Year 1, Task 1, Tasks 2(a)-(c) and Tasks 3(a)-(b) were started and progress was made for each. While experiencing a variety of set backs for each task, I learned a great deal about the experimental process. Additional methods have been identified to further explore Tasks 2(a)-(c) and Tasks 3(a)-(b). The efforts from Year 1 have lead to multiple conference proceedings and journal articles in progress. Furthermore, this grant and data have lead to my successful completion of my preliminary exams.

F. References

[1] C. Archer, M. Tornai, and e. a. JE Bowsher, "Implementation and Initial Characterization of Acquisition Orbits with a Dedicated Emission Mammotomograph," *IEEE Trans Nucl Sci,* vol. NS50, p. 8, 2003.

[2] C. N. Brzymialkiewicz, "Development and evaluation of a dedicated emission mammotomography system," Duke University, 2005., 2005, pp. xxiv, 234 leaves.

[3] M. Tornai, J. Bowsher, C. Archer, J. Peter, R. Jaszczak, L. MacDonald, B. Pratt, and J. Iwanczyk, "A 3D gantry single photon emission tomography with hemispherical coverage for dedicated breast imaging," *Nucl Inst & Meth Phys Res A,* vol. A497, p. 11, 2003.

[4] S. J. Cutler, P. Madhav, K. L. Perez, D. J. Crotty, and M. P. Tornai, "Comparison of reduced angle and fully 3D acquisition sequencing and trajectories for dual-modality mammotomography," in *Nuclear Science Symposium Conference Record, 2007. NSS '07. IEEE,* 2007, pp. 4044-4050

[5] SD Metzler, JE Bowsher, MP Tornai, BC Pieper, J Peter, RJ Jaszczak. 2002. “SPECT Breast Imaging Combining Horizontal and Vertical Axes of Rotation” *IEEE Trans. Nucl. Sci*. **NS-49**(1):31-36.

APPENDIX A: STATEMENT OF WORK

Task 1 Acquire IRB approval to conduct SPECT patient studies and image planar needles (Months 1-6)

a. Participate on writing IRB protocol for FMT imaging in a high risk patient cohort. (Month 1)
b. Modify rpFNA IRB protocol (PI: Seewaldt #4245) to include imaging of planar needles extracted from patient breasts. (Month 1)

Task 2 Evaluate radioactive needles for guided histology (Months 1-36)

a. Design shielded holder or sleeves to image the individual signal from each biopsy needle. (Months 1-3)
b. Construct holder. (Month 4)
c. Use phantoms to test designed holder, and modify as necessary. (Month 5)
d. Obtain 2D image of biopsy needles. (Month 6-36)
e. Analyze the 2D images to determine which needles should be histologically evaluated. (Months 6-36)
f. Determine if there is a statistical correlation between the histology results and the 2D molecular images. (Months 6-36)

Task 3 Optimize patient imaging and biopsy protocol (Months 1-36)

a. Investigate how the dedicated SPECT imaging and biopsy procedures can be optimally integrated to minimize the patient scan times. (Month 1-3)
b. Investigate how the information gained with SPECT imaging can be incorporated into the biopsy procedure. (Months 1-3)
c. Image patients. (Months 6-36)
d. Analyze SPECT studies of returning patients to determine variability in patient setup and image acquisitions. (Months 12-36)

Task 4 Complete other aspects of breast cancer training program (Months 1-36)

a. Shadow a radiologist(s) to observe clinical and diagnostic side in breast cancer imaging (Nuclear Medicine, Mammography). (Months 1-12)
a. Publish research work in peer-reviewed journals. (Months 1-36)
b. Attend and present at local seminars offered at Duke University through Medical Physics and the Breast and Ovarian Oncology Research Program, which is part of the Duke Comprehensive Cancer Center. (Months 1-36)
c. Attend international conferences such as DOD BCRP Era of Hope Meeting, IEEE Medical Imaging Conference, RSNA Conference, Society of Nuclear Medicine or San Antonio Breast Cancer Symposium. (Months 1-36)
e. Prepare and defend thesis. (Months 30-36)

APPENDIX B: CONFERENCE PROCEEDING

Novel Patient Optimized Acquisition Trajectories for Dedicated Breast SPECT Imaging

Kristy L. Perez, *Member, IEEE*, Spencer J. Cutler, *Member, IEEE*, Priti Madhav, *Member, IEEE,* and Martin P. Tornai, *Senior Member, IEEE*

***Abstract*– Novel acquisition trajectories developed for our dedicated breast SPECT camera move 3 dimensionally within a hemispherical volume, fully contouring a patient's pendent breast to provide a high quality, high resolution 3D functional image. Each unique trajectory, created in under a minute, is tailored for each breast of each subject to obtain the highest image quality for a particular study. If a suspected lesion location is known prior to the scan, a trajectory can be created with many close and direct views of the lesion. A torso phantom with an attached 1730 mL breast phantom containing a 2.1 mL (0.8cm radius) spherical lesion was filled with clinical levels of activity: heart:liver:torso:breast:lesion concentration ratio 12:12:1:1:6. A variety of novel acquisition trajectories were employed to image the lesion. Sequentially increasing tilted parallel beam trajectories investigated signals obtained from different polar angles for imaging the breast and chest wall with contamination from the heart and liver. These studies yielded a bound on polar positions for all azimuthal locations in order to minimize background contamination. Other trajectories were created to obtain the best lesion signal. This study shows sinusoidal trajectories can recover the breast's shape and image into the chest wall best. Changing the camera's starting position or subtracting projection views can reduce cardiac and hepatic contamination in the reconstructed image. However, more than one trajectory may provide equivalent image quality. Acquisition trajectories can be created to meet specific imaging goals which consider certain patient factors, such as breast size, lesion location and cardiac and hepatic uptake.**

I. Introduction

The SPECT sub-system of the prototype hybrid SPECT-CT system is capable of moving in fully 3D trajectories such that it can be positioned anywhere within a hemispherical volume encompassing a pendant breast[1-3]. The advantages of these trajectories are that more breast volume and parts of the chest wall can be imaged compared to a simple circular orbit. However, a disadvantage is that the incomplete sampling and overwhelming signals in the heart and liver produce artifacts, potentially distorting the reconstructed images (Fig 1) making them difficult for the radiologist to read.

Manuscript received November 16, 2007. This work has been funded by the National Cancer Institute of the National Institutes of Health (R01-CA096821) and the Department of Defense Breast Cancer Research Program (W81XWH-08-1-0192, W81XWH-06-1-0765 and W81XWH-06-1-0791).

Kristy L. Perez and Martin P. Tornai are with the Medical Physics Program and Radiology Department, Duke University, Durham, NC 27710 USA (telephone: 919-684-7943, e-mail: kristy.perez@duke.edu).

Spencer J. Cutler, Priti Madhav and Martin P. Tornai are with Biomedical Engineering and Radiology Departments, Duke University, Durham, NC 27710 USA.

The objectives of this study are to investigate and minimize the contamination due to direct views of the heart and liver and to maximize the SNR and contrast of a lesion in a pendant breast.

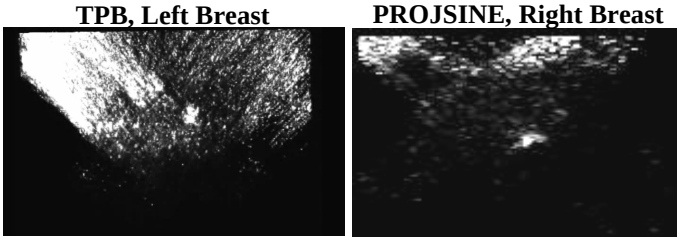

Fig. 1: (LEFT) 2nd iteration MIP image acquired with a tilted parallel beam (TPB) trajectory of a subject showing streak artifacts from incompletely sampled heart and liver activity. The hot-spot at the center is a biopsy confirmed lesion. (RIGHT) 2nd iteration slice image acquired with a projected sinusoidal wave (PROJSINE) trajectory of a subject showing increased activity uptake near the chest wall associated with activity from the heart and liver. The hot-spot near the nipple is a fiducial marker.

II. Materials & Methods

Anthropomorphic phantoms (*RSD, Inc.*, Newport Beach, CA) were filled with clinical concentrations of radioactivity. The heart : liver : torso : breast : lesion activity concentration ratio was 12 : 12 : 1 : 1 : 6. The breast and lesion volumes are 1730 and 2.1 mL, respectively. The torso phantom measures 44 cm wide and 46 cm tall (Fig 2).

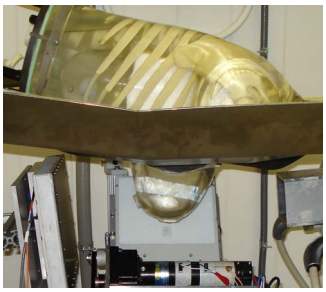

Fig. 2: Anthropomorphic phantoms filled with aqueous solution of ^{99m}Tc radioactivity in clinical concentration ratios. The 1730 mL breast phantom and 2.1 mL lesion phantom are shown here hanging pendant through a hole in our custom built bed and centered in the field of view of the hybrid system. The SPECT-CT system is shown in its normal starting position with the CT source under the patient's head and the SPECT camera on the lateral side of the patient's left breast.

The SPECT system (Fig. 2 & 3) is comprised of a compact 16x20 cm^2 field of view Cadmium-Zinc-Telluride (CZT) *LumaGEM* 3200S^{TM} gamma camera (*Gamma Medica, Inc.*, Northridge, CA) having discretized crystals, each 2.3x2.3x5mm^3 on a 2.5mm pitch. The measured mean energy resolution of the gamma camera at 140keV is 6.7% full-width-

half-maximum (FWHM) and parallel beam collimator sensitivity is 37.9 cps/MBq. The camera is attached to a laboratory jack (model M-EL120, *Newport Corp.*, Irvine, CA) and a goniometric cradle (model BGM200PE, *Newport Corp.*, Irvine, CA) allowing flexible movement through various radii of rotations and 0° to 90° polar tilt angles.

Images are reconstructed with an iterative ordered subsets expectation maximization algorithm. The second iteration with eight subsets per iteration is displayed and used when calculating the SNR and contrast values[2].

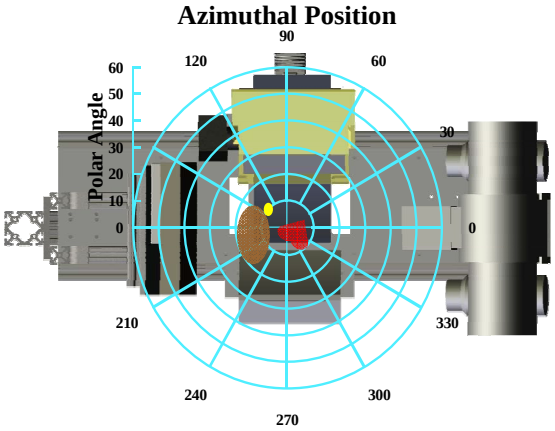

Fig. 3: The red, brown and yellow objects centered on the plot represent relative locations of the heart, liver and lesion, respectively. The SPECT camera is at 90° (gold box) while the CT source is at 0°. The system rotates clockwise and thus the SPECT system images the right upper quadrant

A. Investigating Views of Heart and Liver

Data were acquired with sequential tilted parallel beam (TPB) trajectories (Fig. 4) with polar angles of 15°, 20°, 25°, 30°, 40°, 45°, 50° and 60°. The radius of rotation was varied to approximately contour the breast and 128 projection views were collected for each acquisition. For this data set, the 2.1 mL lesion was placed in the center of the lateral side of the breast (at 90° in the plot in Fig. 4 LEFT). The total counts per projection for each fixed tilt were compared, and qualitative assessments of the reconstructed images were made. The TPB 15° data set is considered to be the "baseline" for the number of counts in the breast and chest wall region. Deviations from the baseline are attributed to additional breast activity as well as activity originating in the heart and/or liver.

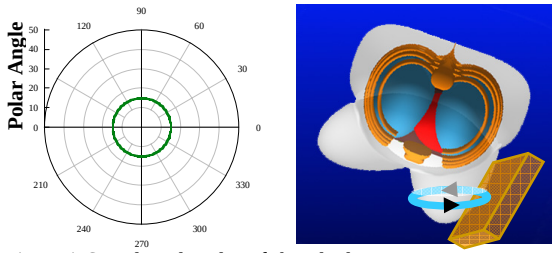

Fig. 4: (LEFT) Sample polar plot of the tilted acquisition trajectory at 15° polar tilt. (RIGHT) 3D rendition of the orbit. The TPB trajectory completes a circle about the central axis of the breast at a fixed tilt.

B. Maximizing SNR and Contrast

The 2.1 mL lesion phantom was placed in the inferior, lateral quadrant of the 1730 mL breast phantom (at 135° in the plot of Fig. 3). In addition to aqueous ^{99m}Tc activity, the breast contained irregularly shaped acrylic pieces and spongy material to displace radioactivity and simulate non-uniform uptake in the breast. One hundred and twenty-eight projection images were collected with a variety of acquisition trajectories (Fig 4 and 5), varying the starting position and polar tilt of some (Table I). The offset starting positions of the trajectories were chosen based on the relative location of the heart and liver identified with the counts per projection from a TPB 45° scout scan. Additionally by knowing the lesion location, trajectories were modified to more closely and directly image that region. The SNR and contrast in the coronal reconstructed slice containing the lesion were used to compare imaging with the different trajectories.

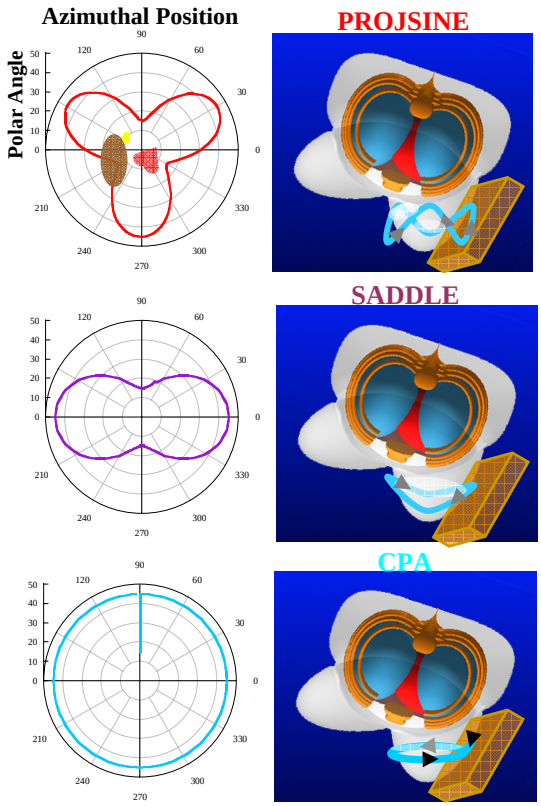

Fig. 5: (LEFT) Polar plot of the acquisition trajectory with its initial position at 90°. (RIGHT) 3D rendition of the trajectory.

TABLE I
TABLE OF DATA ACQUISITION TRAJECTORIES

Trajectory	Initial Position	Polar Range
TPB	90°	0° (No Tilt) 15° 45°
PROJSINE	90° 60° 135°	15° - 45°
SADDLE	90°	15° - 45°
CPA	90° 60° 135°	Arc from 15° - 45° and circle around at 45°

C. Removing Projections to Reduce Heart-Liver Signal

Projection views which deviated from the baseline counts due to signal from the heart and liver were removed and the smaller sub-set of data was reconstructed to compare with the reconstructed full set of data. Images were qualitatively and quantitatively compared. Different acquisitions required a different number of projections to be removed – 17 to 55 projections removed resulting in 47.8° to 154.7° removed – in some cases greatly reducing the total acquisition counts and thus adversely affecting the image quality. However under the assumption that the post-data collection processing would not change the image acquisition procedure, the counts between the full data set and the limited angle data set were not normalized when comparing images.

III. Results & Discussion

A. Investigating Views of Heart and Liver

Figure 6 displays a plot of the counts per projection as a function of azimuthal position. Using TPB 15° as a baseline of normalized contamination-free counts for comparison, there

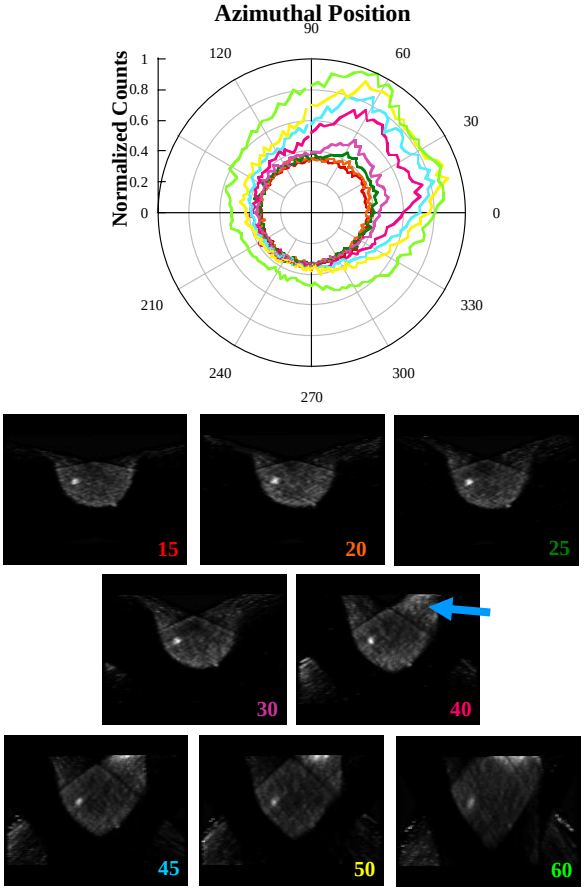

Fig. 6: (TOP) Plot of counts per projection acquired for sequential TPB scans. The plot line color corresponds to the colored tilt angle in the images below. Data are displayed as a solid line. The curves deviate in the upper right quadrant due to increased counts when viewing the heart and liver. (BOTTOM) Three summed transverse slices of second iteration reconstructed images. As the polar angle increases (# in bottom right corner), the imaged volume of the chest wall and axilla increases. The heart and liver activity presents as a bright region (arrow) and shape distortion occurs at ~40°.

are azimuthal positions where large polar tilt angles (40° – 50°) maybe used to image into the chest wall without directly viewing the heart or liver. This indicates that the camera trajectory could encompass large polar angles where the camera might be under the organs and looking up towards the pectoral muscle. Data collected here would not contain direct background counts from the heart or liver. The bounds of the camera's polar angles for the left breast, derived from minima in the counts per projection curve (Fig. 6), shows that the trajectory is most stringently limited in the upper right quadrant (Fig. 7).

Slices from the corresponding reconstructed images show that as the curve deviates from the TPB 15° baseline, increased activity appears in the chest wall region (Fig. 6). The incomplete sampling in these acquisitions manifests itself in the image as breast shape distortion (an elongation and increasingly triangular appearance) and contamination (activity in the lower corners of the images) [1, 2].

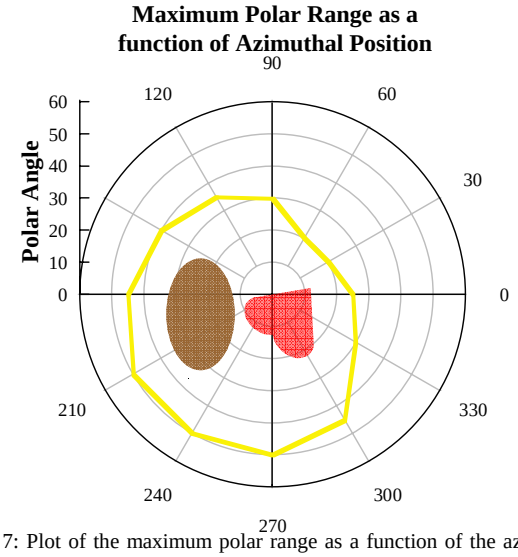

Fig. 7: Plot of the maximum polar range as a function of the azimuthal position for the left breast given minimum (i.e. breast only) counts obtained at these azimuthal and polar views. If the camera trajectory exceeds this range then direct views of the heart and liver will result.

B. Maximizing SNR and Contrast

The reconstructed images in Fig. 8 show the difference resulting from the variety of trajectories used. One trajectory, TPB 45°, which has been proven in patient studies to be an advantageous and useful data collection scheme (Fig. 1 LEFT), surprisingly did not yield a reconstructed image in which the lesion could be visualized. Perhaps if resolution recovery or other corrections were implemented, the lesion might be visualized. However, the other data acquisition trajectories yielded images in which the lesion could be visualized.

The acquisitions which produced the best SNR and contrast (Table II) were the PROJSINE starting at 90° and TPB 15°. CPA starting at 135° had a similarly high contrast, but the SNR was not different than in the other acquired images. The equal SNRs were an unexpected result. Indeed other trajectories, such as PROJSINE starting at 135°, also did not have the high SNR or contrast as expected. While the optimal

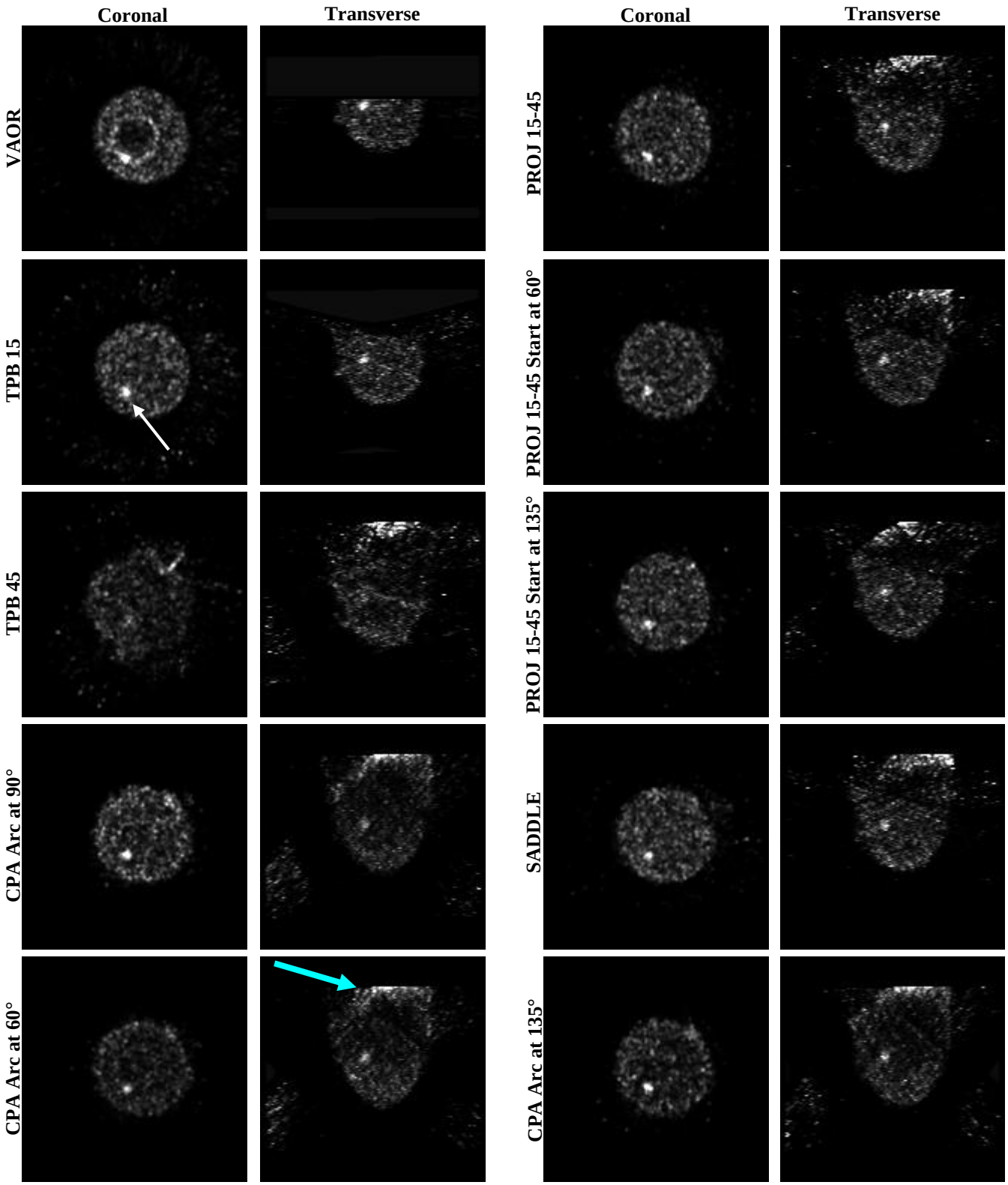

Fig. 8: Four summed second iteration coronal and transverse reconstructed slices smoothed with a Gaussian kernel acquired with a variety of trajectories imaging a 2.1 mL lesion in the inferior, lateral quadrant of a 1730 mL breast phantom. The white arrow points to the lesion location in the TPB 15° image. The aqua arrow points to the increase activity due to the heart and the liver, which is apparent in many of the reconstructed images. Notice: The lesion is not visualized in the image acquired with the TPB 45° trajectory.

acquisition trajectory should have many close and direct views of the lesion, other factors, such as breast size, may warrant consideration in deciding the best trajectory.

TABLE II
TABLE OF SNR AND CONTRAST VALUES IN THE CORONAL PLANE FOR THE SECOND ITERATION OF RECONSTRUCTED IMAGES

Trajectory	SNR	Contrast
VAOR	**3.3**	**4.3**
TPB 15°	**6.2**	**10.7**
TPB 45°	**0.6**	**1**
CPA arcing at 90°	**3.2**	**6.6**
CPA arcing at 60°	**4.8**	**7.4**
PROJSINE	**6.9**	**10**
PROJSINE at 60°	**2.2**	**4**
PROJSINE at 135°	**3.1**	**5.6**
SADDLE	**3.7**	**7.2**
CPA arcing at 135°	**4.8**	**11.4**

C. Removing Projections to Reduce Heart-Liver Signal

Another method to reduce the signal from the heart and liver and use the flexible trajectories of our system is to remove the projection views where the counts deviate from the median counts per projection without contamination. While the activity near the chest wall (presumably from the heart and liver) is reduced with this method, the lesion SNRs and contrasts also decrease (Table III). For this data, the SNRs and contrasts decrease more when more projection views were eliminated, but these views were not close and direct to the lesion which could complicate the procedure. Instead of simply removing the projection from the data set, it could be weighted differently in the iterative reconstruction code, or only the unaffected part of it could be used to avoid the heart and liver signal. Although in the PROJSINE case the number of projections removed was 21 (Fig. 9) and yielded a reasonable reconstruction of the phantom, removing 44 projections for the CPA arcing at 135° (Fig. 10) proved too noisy an image, where the lesion was a little harder to perceive as indicated by the more dramatic decline in SNR and contrast values. If images of equal noise quality were compared, a smaller decrease in SNR and contrast could result and indeed experiments have been conducted for limited angle SPECT studies in our lab[4]. However, the point with this study was to determine if we are able to reduce the cardiac-hepatic effect given our current imaging procedure. Due to the variability in the number of projection views subtracted and the resulting effect on the image quality, this method should not be employed as long as we have the ability to collect the data to avoid the heart and liver.

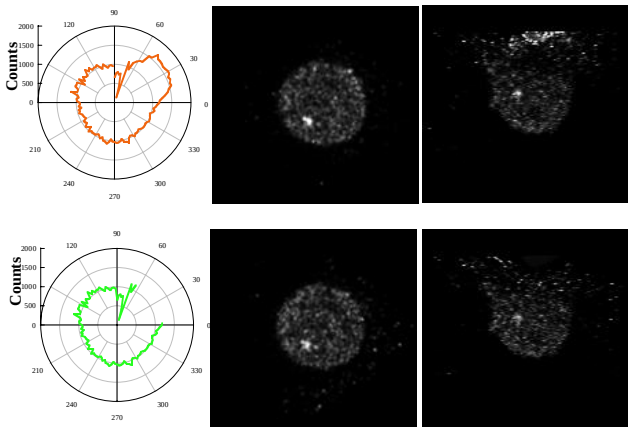

Fig. 9: (LEFT) Plots of counts per projection for the full (TOP) and limited-angle (BOTTOM) PROJSINE acquisitions. The limited-angle case subtracts 21 projection views. The excursion in the plot where the counts drop near 0 was a detector malfunction and is not a true indication of the trend in the data. (RIGHT) Three summed coronal and sagittal slices. Limited-angle images show reduced activity from the heart and liver.

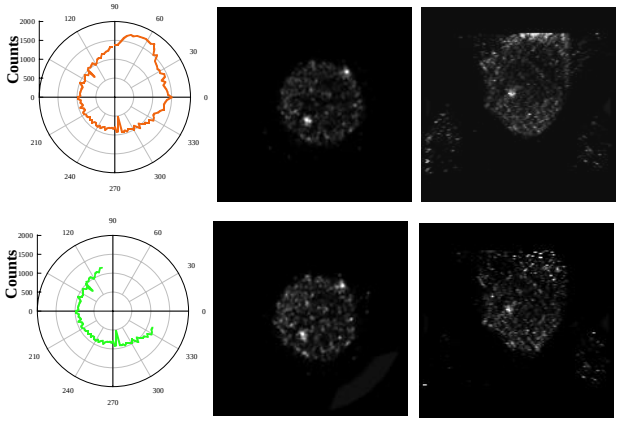

Fig. 10: (LEFT) Plots of counts per projection for the full (TOP) and limited-angle (BOTTOM) PROJSINE acquisition. The limited-angle case subtracts 44 projection views. The excursion in the plot where the counts drop near 0 was a detector malfunction and is not a true indication of the trend in the data. (RIGHT) Three summed coronal and sagittal slices. Limited-angle images show reduced activity from the heart and liver.

TABLE III
TABLE OF SNR AND CONTRAST VALUES IN THE TRANSVERSE PLANE FOR THE SECOND ITERATION OF FULL SET AND LIMITED ANGLE RECONSTRUCTED IMAGES

Trajectory	SNR	Contrast
Full PROJSINE	13.8	6.3
Limited PROJSINE	11.1	4.7
Full CPA arcing at 135°	41.8	18.7
Limited CPA arcing at 135°	17.0	9.7

IV. CONCLUSIONS

Acquisition trajectories can be made to avoid direct views of the heart and liver by limiting the camera's polar angular range over the azimuthal acquisition range (Fig 7). A nearly infinite number of trajectories can be constructed within the

bounds of the maximum polar tilt to avoid the heart and liver and remove the associated artifact while still imaging the lesion. However, for qualitative imaging, a radiologist may be able to "read through" this artifact for lesions located near the nipple as in Fig. 1 LEFT. Therefore, *a priori* knowledge of the lesion location from mammography and breast size (typically smaller than the phantom used here) may affect how much these organs should be considered when setting up an image acquisition and ultimately how much the organs will affect the perceptibility of the lesion. For quantitative imaging, as in previous studies [5], the heart and liver activity would probably need to be accounted for to achieve accurate lesion activity values.

Trajectories can be created to obtain close and direct views of a lesion in a known location, resulting in high SNR and contrast values. Therefore, optimizing an acquisition trajectory to the patient's presentation is possible. Ongoing work in our lab to decrease the setup time by using laser ranging for dynamically controlled breast contouring may be feasible to implement clinically [6]. Future work includes using the maximum polar range data to create acquisition trajectories to fully sample the breast volume while avoiding direct views of the heart and liver.

ACKNOWLEDGEMENT

MPT is the inventor of this imaging technology, and is named as an inventor on the patent for this technology applied for by Duke. If this technology becomes commercially successful, MPT and Duke could benefit financially.

REFERENCES

[1] C. Archer, M. Tornai, and e. a. JE Bowsher, "Implementation and Initial Characterization of Acquisition Orbits with a Dedicated Emission Mammotomograph," *IEEE Trans Nucl Sci*, vol. NS50, p. 8, 2003.

[2] C. N. Brzymialkiewicz, "Development and evaluation of a dedicated emission mammotomography system," Duke University, 2005., 2005, pp. xxiv, 234 leaves.

[3] M. Tornai, J. Bowsher, C. Archer, J. Peter, R. Jaszczak, L. MacDonald, B. Pratt, and J. Iwanczyk, "A 3D gantry single photon emission tomography with hemispherical coverage for dedicated breast imaging," *Nucl Inst & Meth Phys Res A*, vol. A497, p. 11, 2003.

[4] S. J. Cutler, P. Madhav, K. L. Perez, D. J. Crotty, and M. P. Tornai, "Comparison of reduced angle and fully 3D acquisition sequencing and trajectories for dual-modality mammotomography," in *Nuclear Science Symposium Conference Record, 2007. NSS '07. IEEE*, 2007, pp. 4044-4050

[5] SD Metzler, JE Bowsher, MP Tornai, BC Pieper, J Peter, RJ Jaszczak. 2002. "SPECT Breast Imaging Combining Horizontal and Vertical Axes of Rotation" *IEEE Trans. Nucl. Sci*. **NS-49**(1):31-36.

[6] SJ Cutler, DJ Crotty, MP Tornai. "Dynamic Laser-Guided Contouring for Dedicated Emission Mammotomography." *2008 IEEE NSS/MIC*, Dresden, Germany, 19-25 October, 2008.